Aperture edge scatter calibration of the cavity radiometers for the spaceflight Total Irradiance Monitor

David M. Harber, Karl F. Heuerman, Greg A. Kopp, George Lawrence
Laboratory for Atmospheric and Space Physics, Univ. of Colorado
1234 Innovation Dr., Boulder, CO 80303

ABSTRACT

Aperture area knowledge is a primary calibration in radiometric instruments. Corrections for edge effects, particularly diffraction and scatter, must also be taken into account for high accuracy measurements. The Total Irradiance Monitor (TIM) is a total solar irradiance radiometer on NASA's SORCE mission launched in 2003 and on the NASA/Glory mission launching in 2008. In order to measure irradiance, the TIM instrument measures the total optical power that passes through circular diamond-turned precision apertures. The geometric areas of the 8-mm diameter apertures are measured to approximately 25 parts per million (ppm) at the National Institute of Standards and Technology [1]. Due to scatter and diffraction, not all light that passes through the geometric area of an aperture will enter the radiometer cavity of the instrument, and corrections must be made for these edge effects. Diffraction effects are generally well understood and are calculated from the instrument geometry. Scatter, on the other hand, is dependent on the microscopic edge quality of each individual aperture, and so must be measured. This paper describes the measurement of aperture edge diffraction and scatter for the precision apertures on NASA's Glory/TIM instrument.

Keywords: Total solar irradiance, aperture scatter, diffraction

1. INTRODUCTION

The Total Irradiance Monitor (TIM) is an instrument on NASA's Glory mission intended to measure the total solar irradiance to an absolute accuracy of 100 parts per million (ppm), or 0.01%. This instrument is nearly identical to the TIM currently operating on the NASA SORCE mission, launched in 2003. The TIM instrument consists of four electrical substitution radiometers for the measurement of spectrally-integrated optical power [2]. A precision circular aperture of known area is mounted in front of each of these radiometers (see Fig. 1) – this allows the optical power measured by the radiometers to be converted into irradiance. A small correction (430 ppm) must be made for light diffracted by the aperture edge that does not enter the radiometer cavity [3,4]. If the aperture edge contains defects or is of poor quality, then additional light may be scattered into or out of the radiometer cavity. Thus, in order to achieve the planned accuracy of the TIM instrument, the amount of light scattered by the aperture edge must be measured.

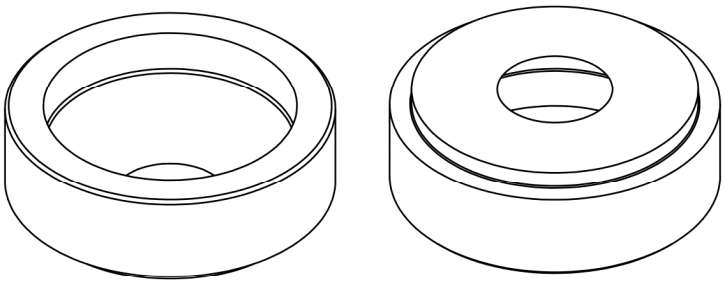

Fig. 1. A drawing of the precision apertures used for the Glory/TIM instrument. The diamond-turned aperture is made from nickel-plated aluminum, and the center aperture diameter is approximately 8 mm. The rear angle of the knife edge (47°) was chosen such that reflections of light external to the instrument off that surface will not enter the radiometer cavities.

Earth Observing Systems XI, edited by James J. Butler, Jack Xiong,
Proc. of SPIE Vol. 6296, 62961I, (2006) · 0277-786X/06/$15 · doi: 10.1117/12.679615

Downloaded from SPIE Digital Library on 14 Feb 2011 to 128.59.62.83. Terms of Use: http://spiedl.org/terms

Diffraction and scatter from the aperture edge are difficult to distinguish experimentally. Incident light is both diffracted and scattered into all angles by the edge, but for small deflection angles the measured signal is dominated by the diffracted component. To discriminate the scattered component, the diffracted component needs to be modeled and subtracted from the total measured intensity.

2. EXPERIMENT

In order to study the light diffracted and scattered from the aperture edge the technique of dark-ground imaging is utilized [5]. In this technique a single lens is used to image the aperture edge onto a CCD camera with both the aperture and the CCD approximately two focal lengths away from the lens. One focal length behind the lens, where collimated light would be focused to a point, is the Fourier plane of the lens. In this plane the angular components of the light incident on the lens are focused to different spatial positions. Using the paraxial approximation, the radial position, *d,* in the Fourier plane is related to the angle of the light incident on the lens, θ (where θ=0 is normal incidence) as:

$$d = f\tan(\theta) \approx f\theta. \tag{1}$$

If different sized beam stops are placed at the on-axis focus in the Fourier plane, different angles of light diffracted and scattered by the aperture edge, which are selectively blocked depending on the size of this beam stop, can be imaged. The measured signal as a function of angle can be compared to models of diffracted light. This allows a good test of the theory used for predicting the diffraction loss of the instrument, and distinguishes between the diffraction and scattered light signals.

2.1. Experiment Setup

The experiment setup is shown in Fig. 2. The illumination source is either a 400 or 627 nm light emitting diode (LED) powered by a constant current laser diode power supply. A diffuser is placed just after the LED, and reduces the angular structure of the LED, producing a nearly uniform illumination of the aperture. The aperture following the LED defines the beam collimation, selected here to match solar collimation (0.53°) at the precision aperture.

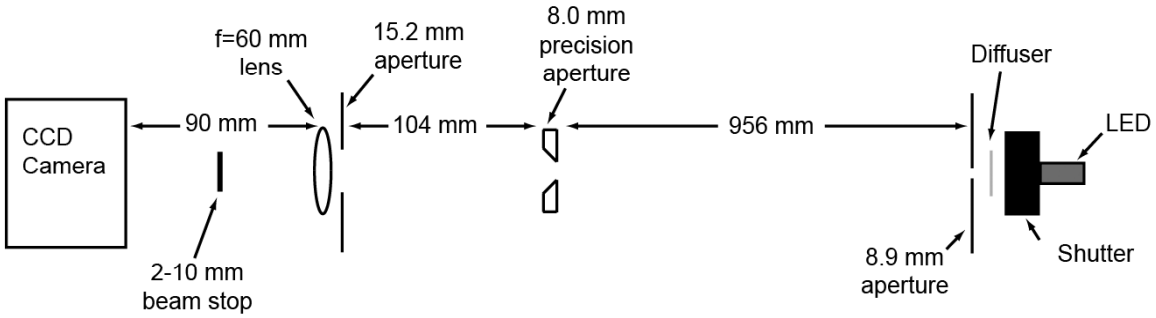

Fig. 2. The basic experiment layout for the aperture edge scatter calibration.

Downloaded from SPIE Digital Library on 14 Feb 2011 to 128.59.62.83. Terms of Use: http://spiedl.org/terms

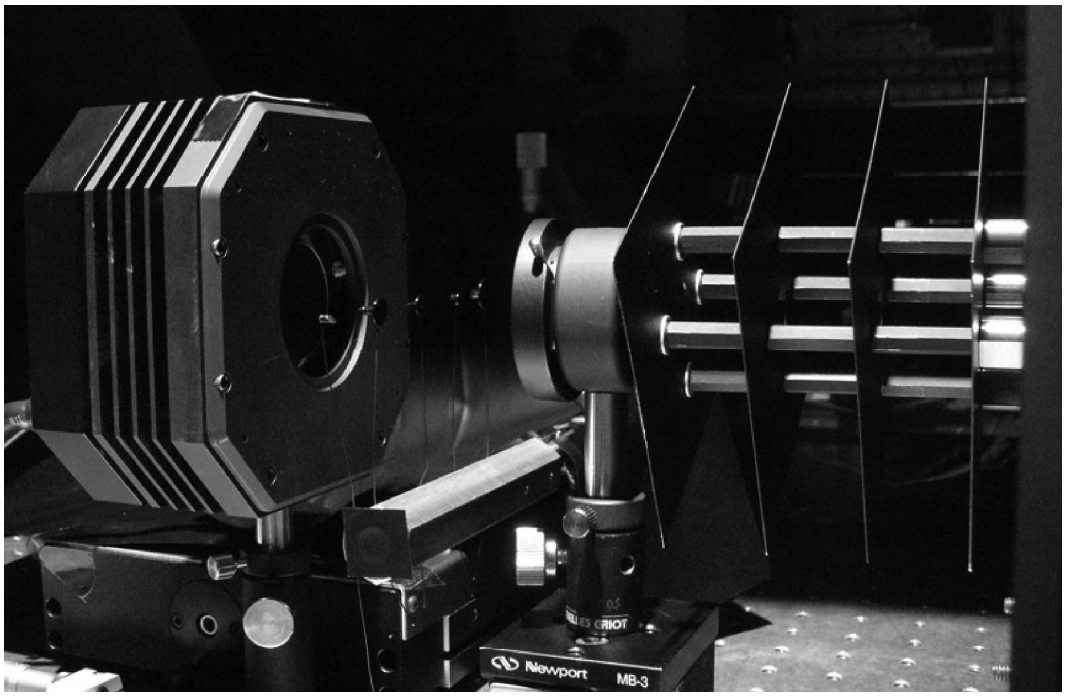

Fig. 3. Image of the experiment showing (from right to left) the baffles following the precision aperture, lens, beams stops, and CCD camera. The five beam stops, visible between the CCD and the lens, are each mounted on a thin piece of wire and fixed to a translation stage for positioning in the beam.

Behind the precision aperture are a series of baffle plates that replicate the baffles in the actual TIM instrument (see Fig. 3). Only the last baffle is shown in Fig. 2. This final baffle is the most critical because it defines the entrance aperture of the radiometer cavity, and thus the field of view of the instrument, while the others reduce far off-axis light. The imaging lens, a f=60 mm focal length achromat, is located just behind the last baffle plate where it effectively collects all light that would enter the TIM radiometer cavity. It is located at a distance of approximately $2f$ behind the aperture edge, and thus will create an image of the aperture edge about $2f$ behind it.

The next component in the experiment setup is the beam stop, which is located in the Fourier plane $1f$ behind the lens. The bulk of the incident light consists of that passing through the aperture undeflected, and so occupies incidence angles from -0.26° to +0.26°. From Eqn. 1, this undeflected light occupies a circle in the Fourier plane with a radius of about 0.27 mm. The maximum angle ray collected by the TIM radiometer, as defined by opposite edges on the precision aperture and the final baffle, is 6.36°. The Fourier plane can thus be illuminated out to a radius of 6.66 mm by diffracted and scattered light from the aperture edge. The purpose of the beam stop is to block the primary, undeflected light, permitting characterization of the much lower intensity scattered and diffracted light. Beam stops with varying diameters allow study of the angular dependence of the scattered and diffracted light. For the results described here, beam stops with diameters of approximately 2, 4, 6, 8, and 10 mm are used.

Downloaded from SPIE Digital Library on 14 Feb 2011 to 128.59.62.83. Terms of Use: http://spiedl.org/terms

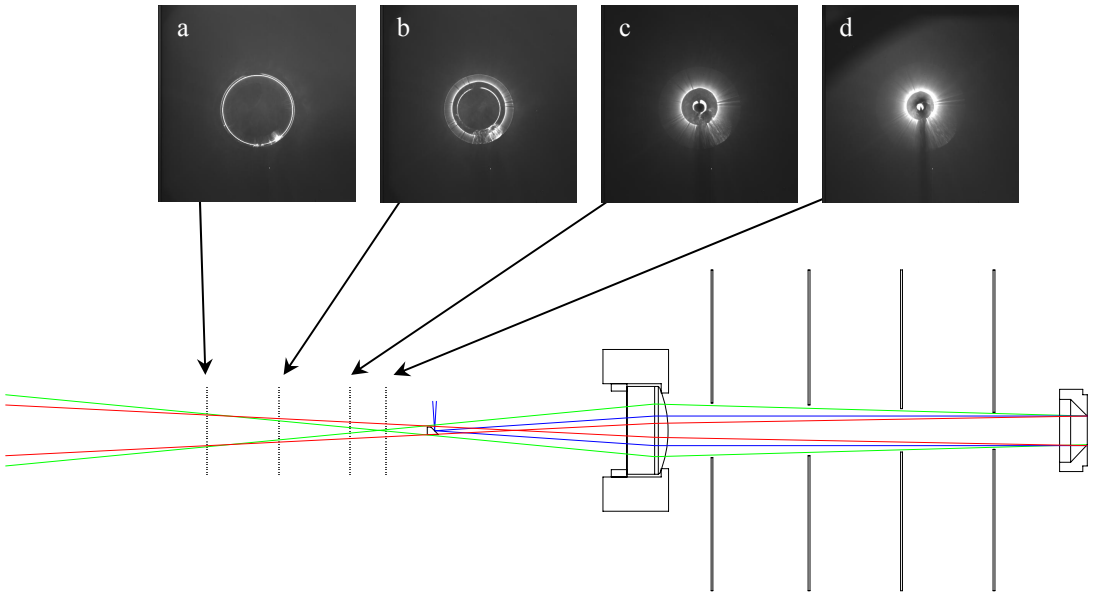

Fig. 4. Images taken by the CCD camera at different on-axis positions with a beam stop in place. (a) The CCD is a distance of $2f$ behind the lens and the image of the aperture edge is nearly in focus. A significant amount of scattered light can be seen from a defect in the lower right part of the aperture edge. (b) CCD is moved closer to the Fourier plane, and two distinct rings are clearly present. The outer ring corresponds to light diffracted towards the optical axis, and the inner ring corresponds to light diffracted away from the optical axis. This is the location used for most of the diffraction and scatter analysis in this paper. (c)-(d) Images taken progressively closer to the Fourier plane. In (d) the wire that is holding the beam stop is visible.

The CCD camera, placed approximately $2f$ behind the lens, allows either the full beam passing through the aperture (with the beam stops removed), or the larger angle scattered and diffracted light (with a beam stop present) to be imaged. With the CCD located at exactly $2f$, the image of the aperture is in focus. With a beam stop present, a ring that corresponds to the light diffracted or scattered from the aperture edge is imaged. For this study, the CCD camera was moved towards the Fourier plane by about 10 mm from the primary focus of the aperture. By working out of focus, two rings are imaged with a beam stop in place, one ring corresponding to the light diffracted or scattered towards the optical axis by the aperture edge, and the other corresponding to light diffracted or scattered away from the optical axis (see Fig. 4).

2.2. Experiment Procedure

A bright-ground image (an image with no beam stop present) establishes the total amount of light passing through the aperture, used for subsequent normalizations of the diffracted and scattered light intensities. Because of the large amount of light this image is acquired with a relatively short exposure time of about 50-100 ms in order to prevent the CCD from saturating. All images are dark corrected by subtracting a dark image where the CCD shutter is opened but the LED shutter remains closed.

The 2 mm beam stop is then moved into place in the Fourier plane using a motorized linear translation stage, and a dark-ground image is acquired at the same LED exposure time as the bright-ground image. A second dark-ground image with the 2 mm stop using an exposure time ~50 times longer (2-3 seconds) gives significantly improved signal-to-noise. The intensities of the short and long exposures are compared to establish a ratio, ρ, that allows intensities of the long exposure image to be corrected to the level of the short exposure image, and thus normalized to the bright-ground image giving the full aperture illumination.

Downloaded from SPIE Digital Library on 14 Feb 2011 to 128.59.62.83. Terms of Use: http://spiedl.org/terms

The other beam stops, with diameters of approximately 4,6,8, and 10 mm are then consecutively positioned in the Fourier plane and an image, using the long exposure time, is acquired. This procedure is performed for each aperture under test at 400 and 627 nm.

2.3. Image Analysis

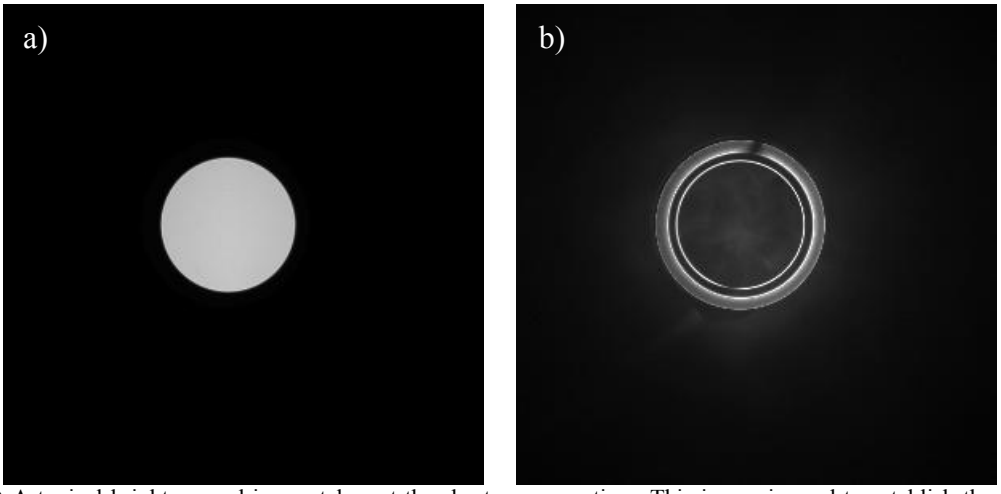

Fig. 5. (a) A typical bright-ground image taken at the short exposure time. This image is used to establish the total light intensity passing through the aperture. (b) A typical dark-ground image with the 2 mm stop in place acquired with the long exposure time. The inner and outer rings respectively show the light deflected away from and toward the optical axis. The faint, indistinct signal in the background is caused by scattering of the intense main beam off defects in the lens, and is subtracted off in the analysis.

Fig. 5 shows typical bright- and dark-ground images. The bright-ground images are simply used to establish the total intensity, I_0, passing through the aperture, computed simply as the sum of all pixels in the image. The dark-ground image, taken with the 2 mm stop as seen in Fig. 5 (b), shows two distinct rings due to the CCD intentionally positioned out of focus; these originate from light diffracted or scatter towards or away from the optical axis.

The long exposure dark-ground images (with a higher signal-to-noise) undergo image analysis in order to determine the total amount of scattered or diffracted light. First an azimuthal average about the center of the aperture is performed, the results of which are shown in Fig. 6 (a). In addition to the two bright rings, a smoothly sloping background is visible. This is caused by scattering of the intense main beam off defects in the lens. To subtract the background, the data outside of the region containing the signal from the aperture edge, as indicated by the diamonds in Fig. 6 (a), is fit by a 5^{th} order polynomial and subtracted from the data, as is seen in Fig. 6 (b). Similarly, this polynomial is used to subtract the background light from the dark field image itself, as is seen in Fig. 7 (b). The integral under each of the two peaks in Fig. 6 (b) is a measure of the total scattered and diffracted light from the edge of the aperture that enters the radiometer at angles sufficiently large so that the light passes by the beam stop. For the 2 mm beam stop this angle is approximately 1.2°.

Downloaded from SPIE Digital Library on 14 Feb 2011 to 128.59.62.83. Terms of Use: http://spiedl.org/terms

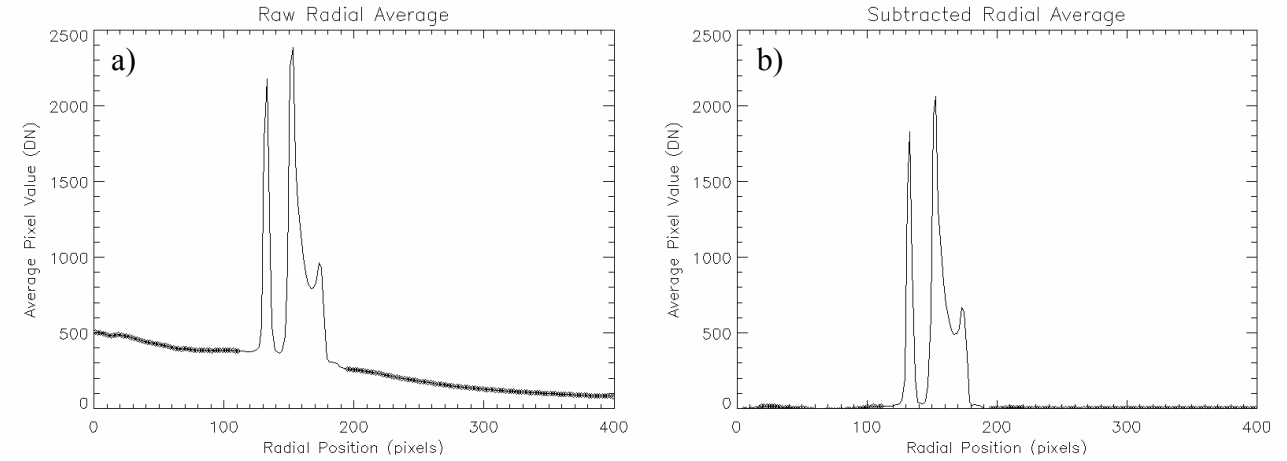

Fig. 6. (a) Azimuthal average of the dark field image from Fig. 5 (b). The smoothly sloping background is caused by light from the main beam scattered from imperfections in the optical components of the system. (b) The same radial average with the background subtracted.

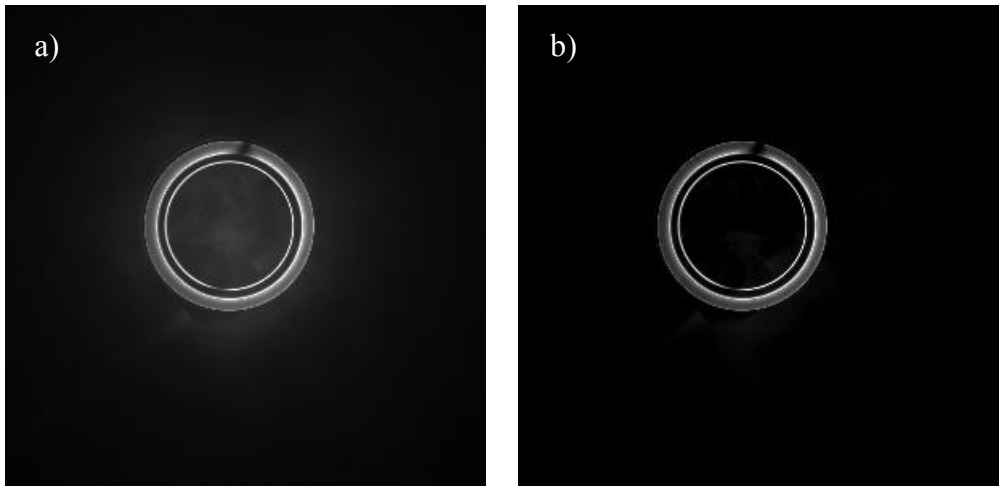

Fig. 7. (a) The dark field image before background subtraction. (b) The same image after the background has been subtracted.

Next, the signal in the inner and outer rings is binned as a function of angle, as is shown in Fig. 8, to show which portions of the aperture circumference contribute to the scatter. Defects in the aperture edge typically correspond with abrupt spatial brightenings in the ring images. The primary residual function is sinusoidal and is caused by alignment errors of the beam stop that increase the amount of light on one side of the stop and reduce it on the other. Thus, to determine the total amount of light in each ring in the absence of the wire support, the data corresponding to points that were not obstructed by the support (as indicated by diamonds) are fit by a sine function (solid line in Fig. 8 (a) and (b)). The sinusoidal component is then subtracted from the data. The total fractional scattered signal in the inner or outer rings can then be obtained from the data shown in Fig. 8 (c) and (d) by simply summing the signal. The total fraction of diffracted and scattered light relative to the total intensity passing through the aperture is then simply obtained by summing the signal in Fig. 8 (c) or (d) and dividing by the total intensity, I_0, and the ratio between the long and short exposures, ρ.

Downloaded from SPIE Digital Library on 14 Feb 2011 to 128.59.62.83. Terms of Use: http://spiedl.org/terms

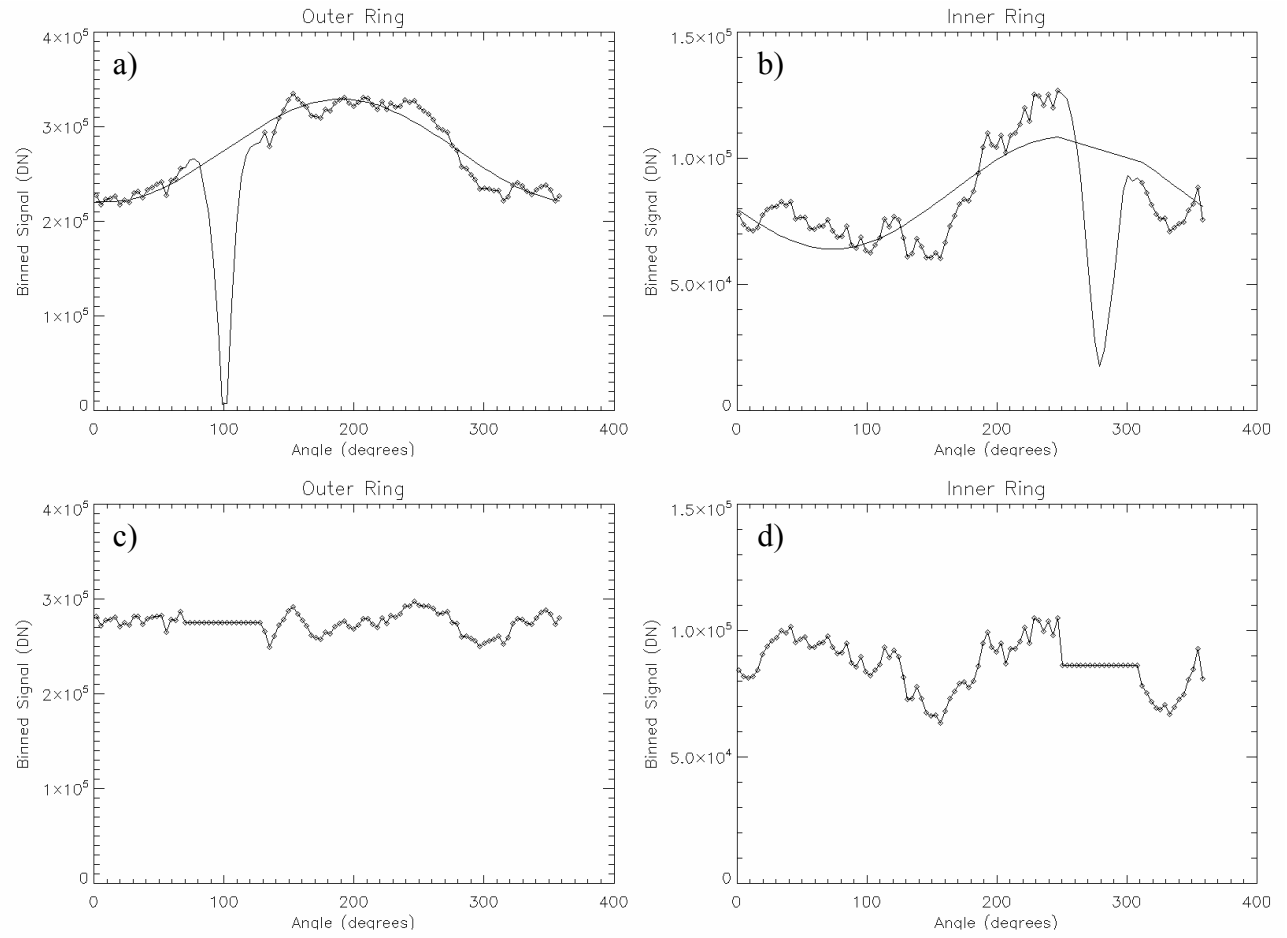

Fig. 8. (a) Integrated signal as a function of azimuthal angle in the outer ring of the image from Fig.6 (b). (b) Integrated signal as a function of azimuthal angle in the inner ring of the image from Fig.6 (b). (c) The signal from (a) with the residual sinusoidal variation removed. The signal over the wire support has been extrapolated. (d) The same technique performed for the data in (b).

3. RESULTS

For each beam stop the amount of diffracted and scattered light that appeared in the dark-field image was measured following the previously described experimental procedure. For the 2 mm stop, which blocked light at angles greater than 1.2°, two distinct diffraction rings were imaged, as was described in Section 2.2. The inner of the two rings originated from light diffracted or scattered away from the optical axis (see Fig. 4). This light was blocked for angles greater than 1.75° by the final baffle. All other beam stops, which blocked light at angles greater than 2°, blocked all of this light, and so for those beam stops only one diffraction ring was imaged.

In Fig. 9 the total measured diffracted and scattered light is plotted for one of the Glory/TIM flight apertures. Additionally, the predicted amount of diffracted light, using Eqn. 9 from Appendix A, is plotted. The agreement between the measured and predicted values indicates that the majority of the measured light is due to diffraction and that the aperture edges create very little scattered light.

Downloaded from SPIE Digital Library on 14 Feb 2011 to 128.59.62.83. Terms of Use: http://spiedl.org/terms

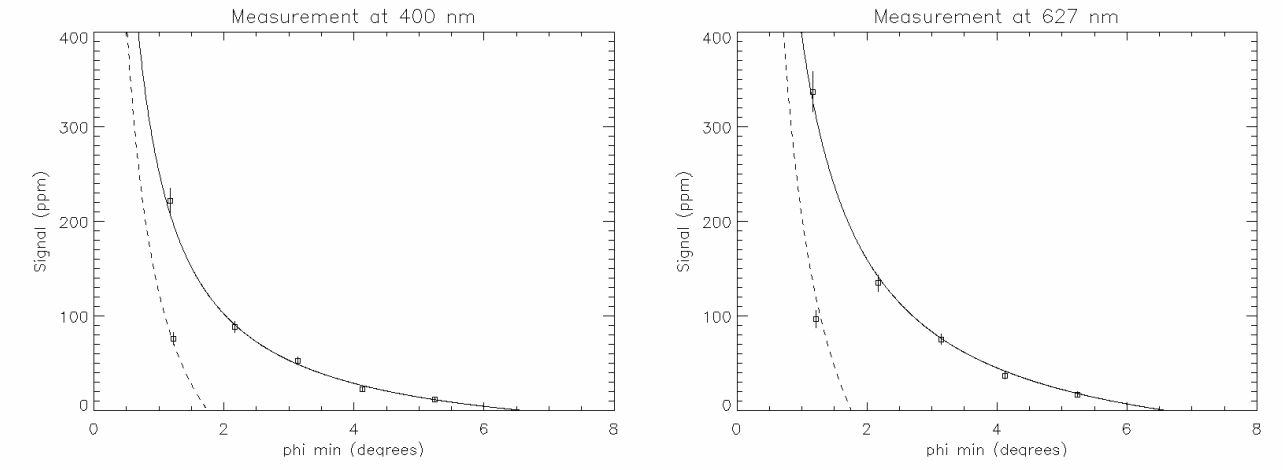

Fig. 9. The measured amount of diffracted and scattered light as a function of $|\phi'_{Min}|$ for one of the Glory/TIM flight apertures (aperture 1). The solid (dashed) line is the predicted amount of diffracted light for $\phi'_{Max} = 6.60°$ ($\phi'_{Max} = 1.75°$) and thus corresponds to the outer (inner) ring in Fig. 7 (b). The agreement between the measured total diffracted and scattered light and the calculated contribution from diffraction alone indicates that very little light is scattered by the edges on the TIM apertures. The diffraction theory from Appendix A may also be used to calculate the amount of light diffracted by the aperture edge that will not enter the radiometer cavity in the TIM/Glory instrument. Performing the calculation at 947 nm, the energy-weighted average wavelength of the solar spectrum, generates a value for the diffraction loss of 453 ppm.

Table 1 summarizes the error budget for the measurement. The geometry uncertainty originates from the uncertainty in the exact diameter and the positioning of the beam stops, and thus propagates to an uncertainty in ϕ'_{Min} and ϕ'_{Max}. The uncertainty in ppm is then estimated through the slope of the calculated diffraction curve in Fig. 9. The LED uncertainty is based on the measured stability of the LED during a timescale on the order of that needed to take the series of bright-ground and dark-ground images. The ratio stability uncertainty is obtained from the variance in the ratio ρ between the long and short exposures. Because the long and short exposure times remain constant, variations in this ratio could, for instance, originate from timing fluctuations of the LED shutter. The uncertainty limit for the CCD linearity was determined by taking a series of bright-ground images with varying exposure times; intensity deviations from linearity with exposure time are used as the limit for the CCD non-linearity. Finally, the background subtraction uncertainty originates from the uncertainty in the 5th order polynomial fit. The total uncertainty differs for each beam stop and is in the range of 2-15 ppm, giving relative measurement uncertainties of ~6-15%.

Table 1. The error budget for the measurement of one of the Glory/TIM flight apertures (aperture 1).

Beam Stop (mm)	Measured Signal (ppm)	Uncertainty (ppm)					
		Geometry	LED Stability	Ratio Stability	CCD Linearity	Background Subtraction	Total
10.16	11.79	1.69	0.06	0.14	0.24	0.24	1.73
8.10	22.18	2.29	0.11	0.27	0.44	0.44	2.39
6.10	52.75	3.12	0.26	0.63	1.06	1.06	3.53
4.01	88.18	4.96	0.44	1.06	1.76	1.76	5.67
2.11	221.53	11.88	1.11	2.66	4.43	4.43	13.74
2.11	76.06	5.63	0.38	0.91	1.52	1.52	6.11

From the plots in Fig. 9 it is clear that there is good agreement between the measurement and the predicted diffraction signal. In Table 2, the calculated integrated χ^2 probability values are shown using the entire dataset of 12 points (6 sets of ϕ'_{Min} and ϕ'_{Max} values at two wavelengths) for the four Glory/TIM flight apertures.

Downloaded from SPIE Digital Library on 14 Feb 2011 to 128.59.62.83. Terms of Use: http://spiedl.org/terms

Table 2. The final results of the aperture edge scatter measurement for the four Glory/TIM flight apertures. All four flight apertures are statistically consistent with no aperture edge scatter.

Aperture Number	χ^2 Probability	Estimated Scatter	Est. Scatter Uncertainty	Aperture Area [1]	Area Uncert. [1]
	%	ppm	ppm	mm^2	ppm
1	45.6	15.1	16.8	50.588615	21.2
2	20.0	1.4	16.8	50.447022	23.6
4	11.7	8.8	16.8	50.321236	21.3
6	27.6	4.1	16.8	50.182467	26.7

From Table 2 we see that the χ^2 probability for the four flight apertures falls within a reasonable range, indicating that the measured signal is statistically consistent with the predicted signal from diffraction alone. To further elucidate the scatter light contribution, we subtracted the contribution due to diffraction from the measurement. Then using an extremely simplified model of scattered light, where the scattered light is assumed to be uniform over the angles and wavelengths of the measurement, we fit the residual data and calculate a contribution due to scattered light. The scattered light estimated in this manner is reported in Table 2. Again, we see that the estimated scattered light is very small, and within statistical uncertainty of zero.

4. CONCLUSION

We have characterized the diffracted and scattered light intensity into the TIM radiometer cavities and compared to diffraction theory. We estimate both the amount of incident light lost due to diffraction and the amount of light scattered into the radiometer cavities for each of the Glory/TIM flight apertures. We find very good agreement between theory-based diffraction estimates and measurements of diffracted plus scattered light, indicating that the primary source of this indirect light is diffraction. We find the edges on the Glory/TIM apertures contribute an insignificant amount of scatter because of their edge quality.

Downloaded from SPIE Digital Library on 14 Feb 2011 to 128.59.62.83. Terms of Use: http://spiedl.org/terms

APPENDIX A. DIFFRACTION CALCULATION

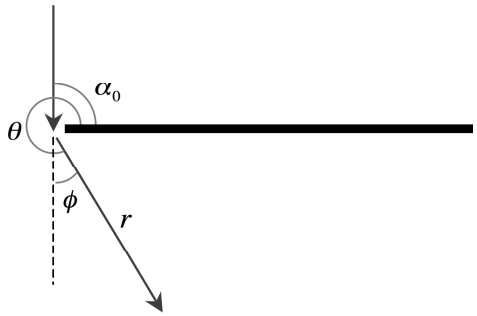

Fig. A-1. The geometry for the calculation of diffraction from a perfectly conducting half-plane.

The dominant contribution to the signal in Fig. 6 (b) is from diffraction. In order to extract the contribution from scattered light, the diffracted light contribution must be calculated. The starting point for this calculation is the exact solution to the diffraction of unpolarized light due to a perfectly conducting half-plane [6] (see Fig. A-1):

$$I(r,\theta) = \frac{I_0}{2}\left[\frac{1}{2} - C(z)\right]^2 + \frac{I_0}{2}\left[\frac{1}{2} - S(z)\right]^2, \tag{2}$$

where C & S are the Fresnel integrals,

$$z = 2\sqrt{\frac{2r}{\lambda}}\sin\left(\frac{\phi}{2}\right), \tag{3}$$

I_0 is the incident intensity, λ is the wavelength of the incident light, r is the distance from the half-plane edge to the point of interest, and ϕ is the angle this light is deflected. In the far-field approximation for $z >> 1$:

$$C(z) \approx \frac{1}{2} + \frac{1}{\pi z}\sin\left(\frac{\pi}{2}z^2\right), \tag{4}$$

$$S(z) \approx \frac{1}{2} - \frac{1}{\pi z}\cos\left(\frac{\pi}{2}z^2\right). \tag{5}$$

Eqn. (2) then becomes

$$I(r,\theta) = I_0\frac{1}{2\pi^2 z^2} = I_0\frac{\lambda}{16\pi^2 r\sin^2(\phi/2)}. \tag{6}$$

Downloaded from SPIE Digital Library on 14 Feb 2011 to 128.59.62.83. Terms of Use: http://spiedl.org/terms

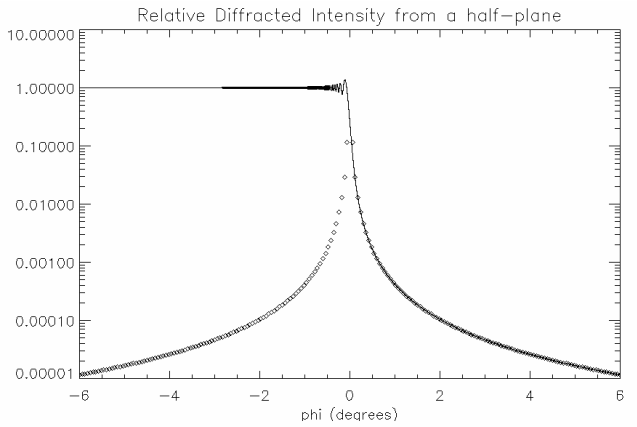

Fig. A-2. The calculated diffracted intensity as a function of angle from a half-plane. The solid line is the exact solution from Eqn. 2. The crosses indicate the approximate solution from Eqn. 6. The approximate solution agrees well with the exact solution for $\phi > 0$. The approximate solution represents only the light diffracted from the edge, sometimes called a boundary wave [7], which is symmetric about $\phi = 0$.

Fig. A-2 shows the exact diffracted intensity and our approximation. Immediately obvious is that the approximation is symmetric about $\phi = 0$; this is because of the assumption $z >> 1$. The diffracted wave is in fact symmetric, so the approximation in Eqn. 6 properly describes the diffracted light for angles other than $\phi \approx 0$.

In order to apply this result to the test situation we would like a form that describes the light diffracted from a circular aperture between two angles. To generate this form we simply multiply Eqn. 6 by the aperture circumference and integrate over the ranges of angles:

$$\frac{I(\phi_{Min}, \phi_{Max})}{I_{Total}} = \frac{\lambda}{4\pi^2 R}\left[\frac{1}{\tan(\phi_{Min}/2)} - \frac{1}{\tan(\phi_{Max}/2)}\right]. \tag{7}$$

This assumes that the radius of curvature of the aperture is much greater than the wavelength of light used.

Next, we consider that the light source is not an infinite distance from the aperture, thus the geometry in Fig. 10 is slightly too simplistic to correctly describe the experiment layout. The most important correction is to allow for non-normal incident light. We can rewrite Eqn. 7 to include a deviation for normal incidence by δ,

$$\frac{I(\phi_{Min}, \phi_{Max})}{I_{Total}} = \frac{\lambda}{4\pi^2 R}\left[\frac{1}{\tan((\phi_{Min} - \delta)/2)} - \frac{1}{\tan((\phi_{Max} - \delta)/2)}\right]. \tag{8}$$

A second smaller effect is that the light source has a finite extent. For a circular light source this can be included by integrating Eqn. 8 over the angular extent of the light:

$$\frac{I_{Diffraction}}{I_{Total}} = \frac{\frac{\lambda}{4\pi^2 R}\int_{-\delta_{Width}}^{\delta_{Width}}\left[\frac{1}{\tan((\phi'_{Min} - \delta)/2)} - \frac{1}{\tan((\phi'_{Max} - \delta)/2)}\right]\sqrt{1 - \frac{\delta^2}{\delta_{Width}^2}}\,d\delta}{\int_{-\delta_{Width}}^{\delta_{Width}}\sqrt{1 - \frac{\delta^2}{\delta_{Width}^2}}\,d\delta}, \tag{9}$$

$$\phi'_{Min} = \phi_{Min} - \delta_{Center}, \quad \phi'_{Max} = \phi_{Max} - \delta_{Center}, \tag{10}$$

where δ_{Center} obtained from the geometry of Fig. A-3 and δ_{Width} is the half-width of the light source (0.26° for this experiment to simulate incident sunlight).

Downloaded from SPIE Digital Library on 14 Feb 2011 to 128.59.62.83. Terms of Use: http://spiedl.org/terms

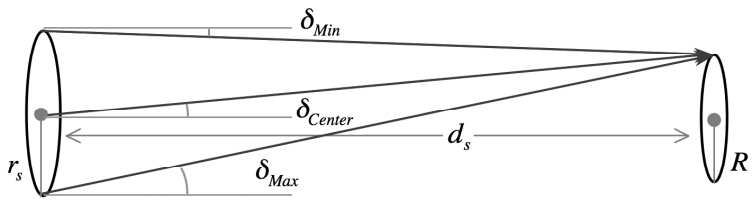

Fig. A-3. The geometry with a finite source size and distance.

REFERENCES

1. J. Fowler and M. Litorja, "Geometric area measurements of circular apertures for radiometry at NIST," *Metrologia*, **40**, S9-S12 (2003).
2. G. Kopp and G. Lawrence, "The Total Irradiance Monitor (TIM): Instrument Design," *Solar Physics*, **230**, 91-109 (2005).
3. G. Kopp, K. Heuerman, and G. Lawrence, "The Total Irradiance Monitor (TIM): Instrument Calibration," *Solar Physics*, **230**, 111-127 (2005).
4. E. L. Shirley, "Revised formulas for diffraction effects with point and extended sources," *Applied Optics*. **37**(28), 6581-6590 (1998).
5. J. W. Goodman, *Introduction to Fourier Optics*, pg. 222, Roberts & Company, (2005).
6. M. Born and E. Wolf, *Principles of Optics*, pg. 656, Cambridge University Press, (1999).
7. S. Ganci, "Boundary diffraction wave theory for rectilinear apertures," *Eur. J. Phys*. **18**, 229-236 (1997).

Downloaded from SPIE Digital Library on 14 Feb 2011 to 128.59.62.83. Terms of Use: http://spiedl.org/terms